Bioactive Materials 1 (2016) 151–159

Contents lists available at ScienceDirect

Bioactive Materials

journal homepage: http://www.keaipublishing.com/en/journals/bioactive-materials/

Akermanite used as an alkaline biodegradable implants for the treatment of osteoporotic bone defect

Wenlong Liu [a, d], Ting Wang [a, b], Xiaoli Zhao [a], Xiuli Dan [c], William W. Lu [d], Haobo Pan [a, *]

[a] Research Center for Human Tissue and Organs Degeneration, Institute of Biomedicine and Biotechnology, Shenzhen Institutes of Advanced Technology, Chinese Academy of Sciences, Shenzhen, China
[b] Shenzhen Key Laboratory for Innovative Technology in Orthopaedic Trauma, Department of Orthopaedics, The University of Hong Kong-Shenzhen Hospital, University of Hong Kong, Shenzhen, China
[c] School of Biomedical Sciences, Faculty of Medicine, The Chinese University of Hong Kong, Hong Kong
[d] Department of Orthopaedics and Traumatology, Faculty of Medicine, The University of Hong Kong, Hong Kong

ARTICLE INFO

Article history:
Received 10 September 2016
Received in revised form
16 November 2016
Accepted 16 November 2016
Available online 7 December 2016

Keywords:
Osteoporotic bone defect
Akermanite
Material-bone interface
Microenvironment pH

ABSTRACT

In osteoporosis scenario, tissue response to implants is greatly impaired by the deteriorated bone regeneration microenvironment. In the present study, a Mg-containing akermanite (Ak) ceramic was employed for the treatment of osteoporotic bone defect, based on the hypothesis that both beneficial ions (*e.g.* Mg^{2+} *ect.*) released by the implants and the weak alkaline microenvironment pH (μe-pH) it created may play distinct roles in recovering the abnormal bone regeneration by stimulating osteoblastic anabolic effects. The performance of Ak, β-tricalcium phosphate (β-TCP) and Hardystone (Har) in healing a 3 mm bone defect on the ovariectomized (OVX) osteoporotic rat model was evaluated. Our results indicated that, there's more new bone formed in Ak group than in β-TCP or Har group at week 9. The initial μe-pHs of Ak were significantly higher than that of the β-TCP and Blank group, and this weak alkaline condition was maintained till at least 9 weeks post-surgery. Increased osteoblastic activity which was indicated by higher osteoid secretion was observed in Ak group at week 4 to week 9. An intermediate layer which was rich in phosphorus minerals and bound directly to the new forming bone was developed on the surface of Ak. In a summary, our study demonstrates that Ak exhibits a superior bone regenerative performance under osteoporosis condition, and might be a promising candidate for the treatment of osteoporotic bone defect and fracture.

1. Introduction

Osteoporosis is a multifactorial skeletal disease characterized by low bone mass with deteriorated bone microstructure [1]. Compared with normal bone, the regeneration process of osteoporotic bone defect was strongly impaired due to the weaker capability of bone formation than bone resorption. Therefore, in the application of biomaterials to osteoporotic patients, a proper physical support together with the function to ameliorate the unbalanced regeneration microenvironment are strongly recommended [2].

Among various influencing factors, the *in vivo* microenvironment pH (μe-pH) has been demonstrated to be important in the bone defect rehabilitation process [3–5]. According to our previous studies, the detection of μe-pH was realized by using a pH microelectrode, and the results indicated the μe-pHs of our specifically tested biomaterials were significantly different from the homogeneous peripheral blood pH and exhibited unique changing patterns with time. The alkaline biodegradable material showed promising healing effect in the context of osteoporotic bone defects [5]. Besides, we realized that the μe-pH generated by implant biodegradation may be influenced by the release of surface ions, such as Si^{4+}, Mg^{2+}, and Zn^{2+}, so that a similar μe-pH could be generated through a combination effect of different released ions. Although the beneficial effects of these ions have been widely reported [6–9], the regulation and function of the *in vivo* μe-pH change, according to our literature review, are still remained to be further discussed.

* Corresponding author.
E-mail address: hb.pan@siat.ac.cn (H. Pan).
Peer review under responsibility of KeAi Communications Co., Ltd.

http://dx.doi.org/10.1016/j.bioactmat.2016.11.004

Calcium silicate ($CaSiO_3$, CS) is celebrated for its bioactivity, osteoinductivity and biodegradability which could grant a better bone regenerative capacity than β-tricalcium phosphate (β-$Ca_3(PO_4)_2$, β-TCP) [10,11]. However, the problem of high dissolution rate limits the application of CS as an orthopaedic implants [12]. A Ca–Mg/Zn–Si bioceramic system generated by incorporating magnesium/zinc into silicate based framework (*e.g.* akermanite ($Ca_2MgSi_2O_7$, Ak), diopside ($CaMgSi_2O_6$), hardystonite ($Ca_2ZnSi_2O_7$, Har) *ect.*) are expected to exhibit a more controllable degradation rate [13] and suitable mechanical properties [14] for applications as orthopaedic biomaterials. *In vitro* study revealed that adipose-derived stem cells and osteoblasts presented better proliferation and osteogenesis behavior on akermanite than on β-TCP [15,16]. Consistently, a faster new bone formation rate derived from non-osteoporotic rabbit femur bone defect was observed in akermanite porous bioceramic than in β-TCP [17]. A recent research further proved that akermanite showed promotion effects on angiogenesis while suppress osteoclastogenesis for osteoporotic bone regeneration [18].

However, although the combination effect of Mg^{2+} and Si^{2+} in akermanite on osteogenesis under osteoporotic condition has been reported, to our knowledge, there's currently a lack of study that is focused on the evaluation of the *in vivo* μe-pH change influenced by the release of these ions. Besides, knowledge of element distribution of Ak in microenvironment between implant and new bone is still in deficiency. In this study, a Mg-containing akermanite has been fabricated and applied under osteoporotic bone defect regeneration condition, combining the repair capacity of beneficial ions and alkaline μe-pH. The simulative effect of akermanite on new bone was examined by an OVX rat tibia defect model, and the interfacial elements distribution between implant and new bone was examined by energy-dispersive X-ray spectroscopy (EDX) linear scanning.

2. Materials and methods

2.1. Materials characterization

Akermanite ($Ca_2MgSi_2O_7$, Ak), Hardystone ($Ca_2ZnSi_2O_7$, Har), and beta-tricalcium phosphate (β-$Ca_3(PO_4)_2$, β-TCP) were kindly provided by Shanghai Institute of Ceramics, Chinese Academy of Sciences. Briefly, akermanite and hardystonite were fabricated by sol–gel process with raw materials of tetraethyl orthosilicate ($(C_2H_5O)_4Si$), magnesium/zinc nitrate hexahydrate ($Mg(NO_3)_2\cdot 6H_2O$/$Zn(NO_3)_2\cdot 6H_2O$) and calcium nitrate tetrahydrate ($Ca(NO_3)_2\cdot 4H_2O$) [17]. β-TCP was prepared by the reaction of $Ca(NO_3)_2\cdot 4H_2O$ with $(NH_4)_2HPO_4$ [10]. All materials were ground and sieved to 300–450 μm (irregular shape), and sterilized by gamma irradiation (270 Gy) before use. The nature of the tested materials used in this study was confirmed by X-ray diffraction (XRD) spectrum with a D8 Advance (Bruker, Billerica, MA, USA). The 2θ was set from 10° to 80°.

2.2. Animal model

2.2.1. Osteoporotic rat model

All animal surgical procedures were conducted under protocols approved by the Committee on the Use of Live Animals in Teaching and Research, The University of Hong Kong (CULATR No. 2572-11; 2555-11). Female Sprague-Dawley rats aged 10 months were chosen in this study. Osteoporosis was inducted by ovariectomy (OVX) surgery as previously described [19,20]. Briefly, after anesthetization, an incision was made at the midline of the abdomen through which both ovaries were excised bilaterally; bleeding control procedures were instituted and the incision was sutured. Bone mineral density (BMD) of the proximal tibia was measured by Micro-computerized tomography (CT) (Skyscan 1076, Skyscan, Kontich, Belgium). 3 months after OVX surgery, osteoporotic rat model was successfully established.

2.2.2. Material implantation

A secondary surgery was performed three months after the OVX surgery, bilateral bone defects were created in the median aspect of the tibial shaft, below the tibial plateau. Briefly, incisions were made bilaterally after shaving and aseptic procedures on the median aspect of the proximal tibia. Defects with depth and diameter of 3 mm were created with a 3-mm drill at low speed. Both defects were then packed gently with each material powders (Ak, Har or β-TCP) with four replicates for each time point. After μe-pH detection, the entrance of the defect was sealed using bone wax (Ethicon, Somerville, NJ, USA) and the skin was sutured (Ethilon, Ethicon). Blank controls were treated similarly but without material implantation. Antibiotic (Baytril®, Enrofloxacin, Bayer HealthCare, Kiel, Germany) was administered in the drinking water for 3 days. Rats were euthanized with an overdose of pentobarbital (Alfasan; 150 mg/kg) at 1, 4 or 9 weeks. Both tibiae were then harvested.

2.2.3. Detection of in vivo μe-pH

The pH meter was normalized before use (Model 60, Jenco, San Diego, CA, USA), and the μe-pH was determined immediately after materials implantation. The sensing tip of the microelectrode (MI-413P, Microelectrodes, Bedford, NH, USA) was placed on the surface of the blood-saturated packed powder, and the stable value of the initial detection was used for analysis. Protein contamination on the sensor was removed after each measurement by immersing the sensor in enzymatic detergent (Tergazyme, Alconox, White Plains, NY, USA). Before tissue was harvested, the bone wax was removed, the surface layers of the implants were carefully scraped with a scalpel to expose the implant fully, and thus its internal microenvironment, for its μe-pH to be measured again in the same way.

2.3. Evaluation

2.3.1. Micro-CT analysis

The implantation sites were scanned by Micro-computerized tomography (CT) at a voltage of 88 kV and current of 100 μA. The rotation step was 0.6° and the isotropic voxel size was 17.33 μm. Data was reconstructed by software (NRecon Server, version 1.6.6.0, Skyscan). A column of 0.4 × 1.0 mm^2 (height × radius) in the center of the implantation site was chosen as the volume of interest (VOI). According to our results, the X-ray attenuation coefficient (AC) of rat trabecular bones was lower than 25.1 m^{-1}, so that objects with an AC higher than 25.1 m^{-1}, which were chosen as the object of interest, can be identified as the remaining implant. Volume of object in VOI (Obj.V/TV) and relative surface area (Obj.S/Obj.V) were calculated by software (CT Analyser, V. 1.10.0.1, Skyscan). The 3D VOI images at time points of week 1, 4 and 9 were created based on AC (CT Vol, version 2.1.0.0, Skyscan).

2.3.2. Decalcified histology staining

Harvested tibias were processed for standard procedures of fixation, ethylene diamine tetraacetic acid (EDTA) decalcification, dehydration and paraffin-embedding [21]. Five-micrometer sections were created for histological staining (haematoxylin and eosin, Sigma–Aldrich) to detect the specific tissue response to the implanted materials. Semi-quantitative examinations for new bone formation were analyzed by 8 parallel samples, and the histogram was established by software (GraphPad Prism 5, La Jolla, CA, USA).

2.3.3. Undecalcified histology staining

Undecalcified samples were prepared with similar methods applied to decalcified tissue but without EDTA treatment. Samples were infiltrated, embedded with methyl methacrylate (MMA) (Merck) and cut into 200 μm sections with a low-speed saw (Iso-Met, Springfield, VA, USA) in running water. Sections were subsequently polished to about 50 μm thickness (model 310 CP band system, Exakt). Osteoid formation capability was examined by goldner's trichrome staining, while toluidine blue staining was utilized to distinguish the junction between the implant and new bone [21].

2.3.4. Elemental analysis

An energy-dispersive X-ray spectroscopy (EDX) detector (EMAX, EX-350, Horiba, Tokyo, Japan) on a scanning electron microscope (SEM) (S-4800 FEG, Hitachi, Tokyo, Japan) was used to assess elemental distribution development over time. Elemental distributions from the original implant sites to the newly formed bone sites at different time points were conducted on 200 μm paraffin-embedding sections acquired from undecalcified histology processing step. The sections were carbon-sputtered, and were linear or area scanned at an operating voltage of 20 kV. The distribution and constitution of Mg/Zn, Ca, P and Si on the surface of sections were subsequently identified. An average of three repetitions of each scanning were recorded and analyzed in software (INCA Energy software, Oxford Instruments, Abingdon, Oxfordshire, UK).

2.4. Statistical analysis

Quantitative results were expressed as the mean ± standard deviation (SEM). Shapiro-Wilk and Levene tests were performed to check the normality and the homogeneity of the variance. Parametric analysis was carried out by using one-way analysis of variance (1 way ANOVA) followed by a LSD post-hoc multiple comparisons. All statistical analyses were conducted in software (SPSS Statistics for Windows 17.0, SPSS, Chicago, IL, USA). The critical value was set at $\alpha = 0.05$.

3. Results

3.1. Material characterization

XRD patterns of the prepared materials were presented in Fig. 1. The diffraction peak for β-TCP (whitlockite, syn), Ak and Har, which were referred to their powder diffraction file card (*i.e.* PDF card # for β-TCP: 09-0169; Ak: 35-0592 and Har: 35-0745), were identified respectively. The incorporation of Mg/Zn into the calcium silicate framework was further confirmed by the EDX scannings from tissue sections acquired *in vivo* studies (Supplementary Fig. 1).

3.2. In vivo μe-pH variation

As illustrated in Fig. 2, the *in vivo* μe-pH changing data acquired from the initial detection with a pH microelectrode were recorded. After implantation, *in vivo* μe-pHs for β-TCP, Ak and Har were increased immediately in comparison with the blank group (7.39 ± 0.03), with Ak (7.82 ± 0.04) and Har (7.80 ± 0.04) giving a significantly higher value compared with β-TCP (7.68 ± 0.04) ($P < 0.05$), that was Ak ≈ Har > β-TCP > Blank. After that, the μe-pH of Ak and β-TCP decrease slightly at time point of week 1 and then increased gradually from week 1 to week 4; whereas the μe-pH of Har dropped significantly to a minimum (7.65 ± 0.01) at week 1, and then maintained at that relative constant level (7.65–7.71) throughout our detection period. The μe-pH values of the tested materials were higher than the blank at all examined time points, whereas the significant difference among all types of materials faded at week 9.

3.3. Implants biodegradation

Threshold attenuate coefficient of 25.1 m^{-1} was chosen to distinguish new bone from the remaining materials. Compared with the condition at week 1, Ak powders (with a AC higher than 25.1 m^{-1}) lost almost two third of its initial volume after 9 weeks implantation; whereas the relative surface area of these materials (Obj.S/Obj.V) was increased gradually during this process (Fig. 3

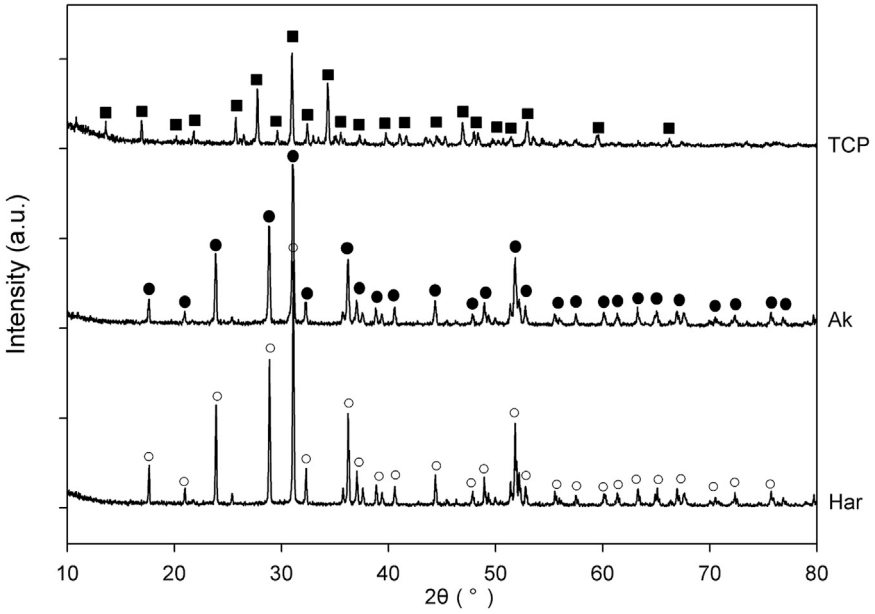

Fig. 1. XRD patterns of the prepared β-TCP, Ak and Har. Diffraction peaks were labeled "■" for β-TCP (PDF card #: 09-0169), "●" for Ak (PDF card #: 35-0592); and "○" for Har (PDF card #: 35-0745).

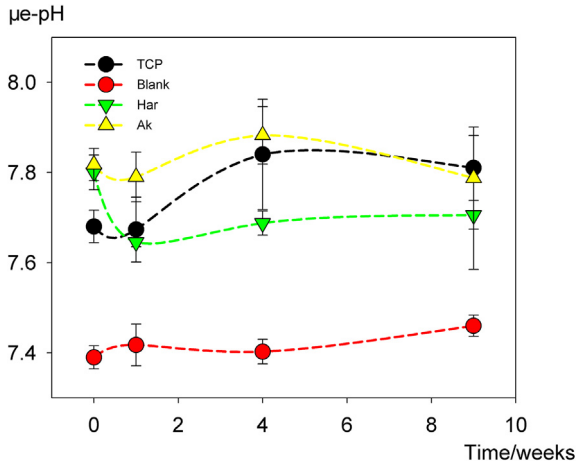

Fig. 2. Variation of μe-pH with time post-implantation. Data were expressed as mean ± SEM, n=4.

AB). The changing tendency of Obj.S/Obj.V and Obj.V/TV through time was reversed, and this may be attributed to that the new bones (or intermediate mineral layer) which formed on the surface of the implants attenuated their further degradation. Compared with Ak, significantly higher Obj.V/TV, but a relatively lower Obj.S/Obj.V was observed in both β-TCP and Har group at week 9.

3.4. New bone formation

Chronologically, after implantation, Ak powders were encapsulated by fibrous tissues (Fig. 4; Ak-1W, "F") which were then gradually substituted by bone marrow (Fig. 4; "BM") from week 1–4. The new bone matrix (stained in pale pink) could be clearly observed on the surface of Ak at the time point of week 4 (Fig. 4; "NB"), and it was increased significantly at week 9. As indicated by our results, β-TCP exhibited good osteoconductive property, while the fibroblastic response in Har group can be still observed at 9 weeks post-surgery. The semi-quantitative results (Fig. 4; bottom) indicated that the new bone content in Ak group was significantly higher than that in either β-TCP or Har group at week 9 ($P < 0.05$).

3.5. Goldner's trichrome staining for osteoid

As shown in Fig. 5, the calcified new bone regions were stained in green, while new osteoid in red. New osteoids were traceable on the surface of Ak as early as week one, and were then gradually replaced by mineralized mature bone. Increased osteoid areas, indicating increased osteoblast activity, were observed conspicuously in Ak at week 9, in comparison with β-TCP (Fig. 5; Ak-9W,

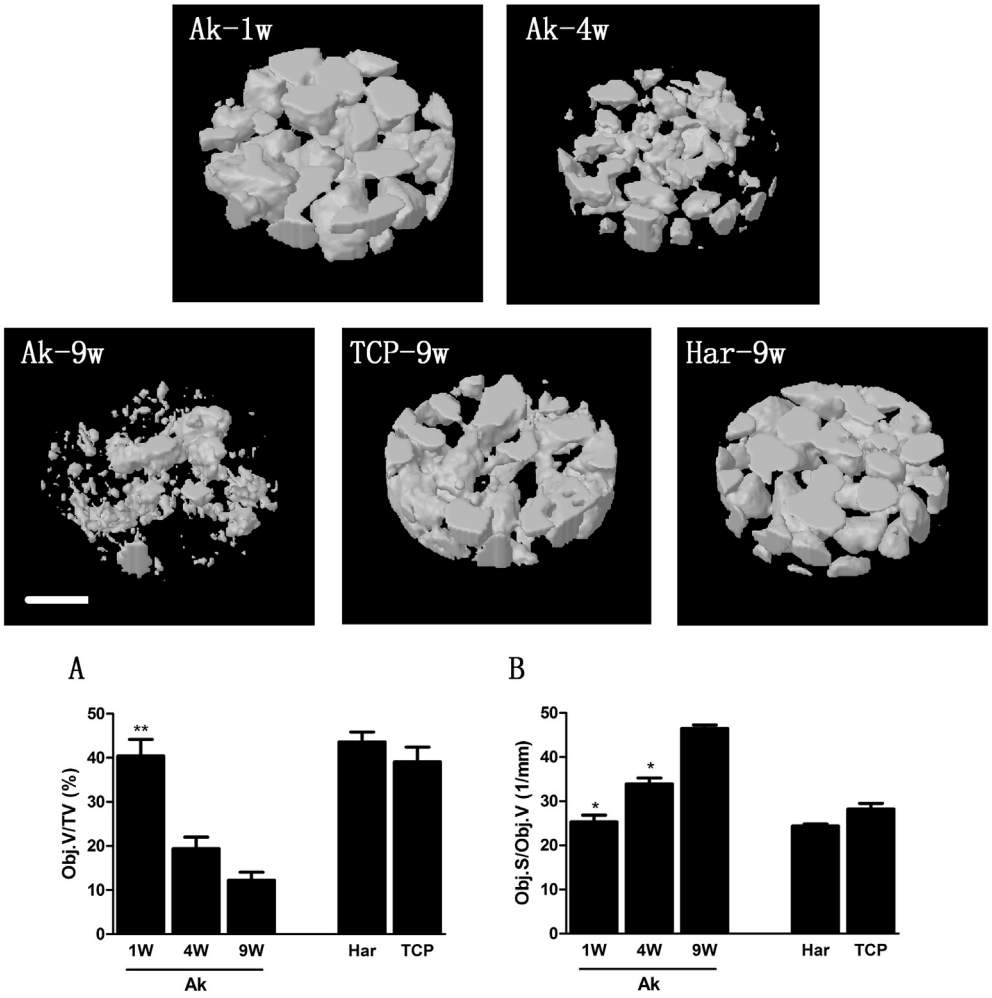

Fig. 3. 3D reconstructed images of the volume of interests (VOI) (threshold AC = 25.1 m^{-1}) during the osteoporotic bone defects regeneration process. Variation of the remaining minerals (Obj.V/TV) (A) and relative surface area (Obj.S/Obj.V) (B) within VOI were parameters of interest (Mean ± SEM; n = 4; $p < 0.05$ (*)). Scale bar: 0.5 mm.

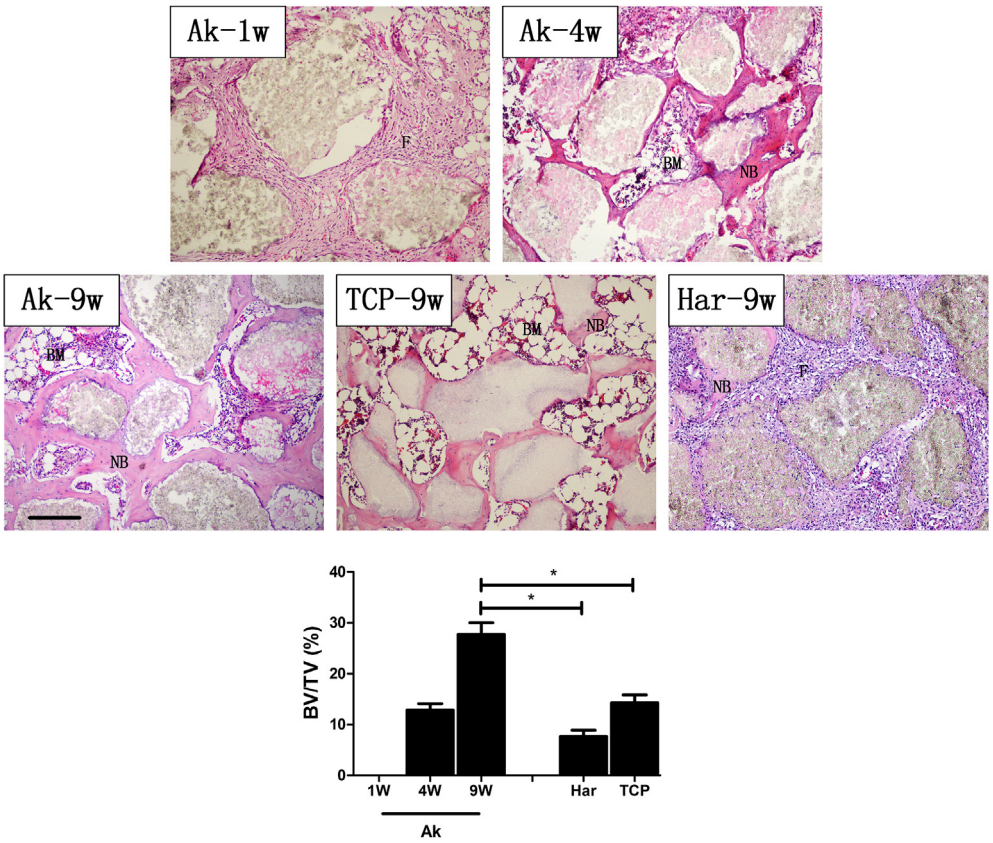

Fig. 4. H&E staining during the osteoporotic bone defect healing process. New bone (NB) was stained in pink/pale-pink; bone marrow was marked "BM"; fibrous tissues were marked "F". Scale bar: 200 μm. Semi-quantitative results for new bone volume/tissue volume ratio (BV/TV) in each group at different time points was listed at the bottom. (Mean ± SEM; n = 8; $p < 0.05$ (*)).

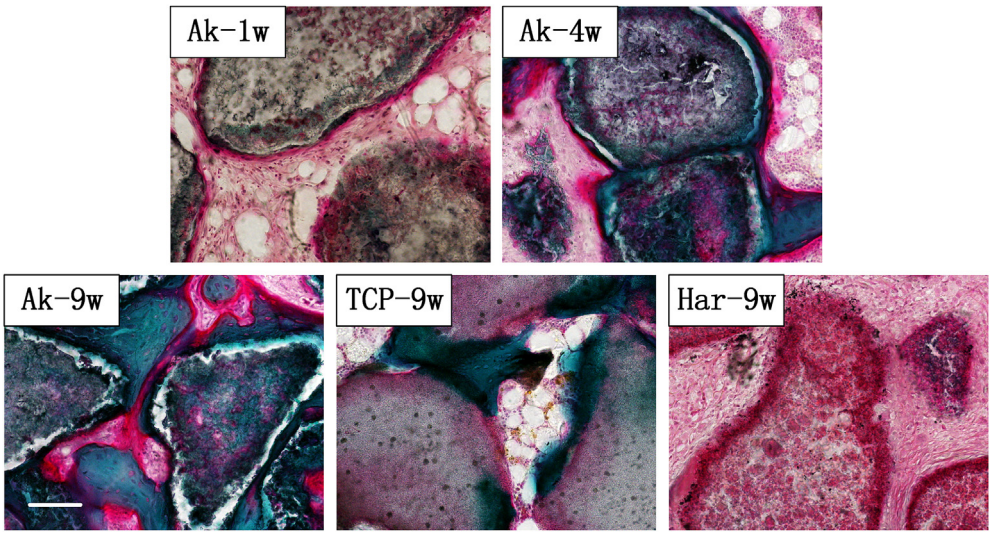

Fig. 5. Undecalcified goldner's trichrome staining during the osteoporotic bone defect regeneration process. New osteoid was stained red; calcified bone was stained dark green. Scale bar: 100 μm.

TCP-9W). According to our results, new bones that formed on the surface of Har were less mineralized bone in comparison with the other two groups.

3.6. Interface of material-bone junction

As shown in Fig. 6, osteocyte lacunae can be observed in new bone area. Margin of original material regions were partially stained in blue (M'), leaving the centre of the material pale in color (M). The majority of locations originally resided by Ak were occupied by an intermediate (assumed apatitic) calcium phosphate M' layer afterwards (Fig. 6; Ak-4w, Ak-9w). In consistent with Fig. 4, new bone formed on the surface of intermediate M' layer in Ak group, and increased in area with time. The outline between M and

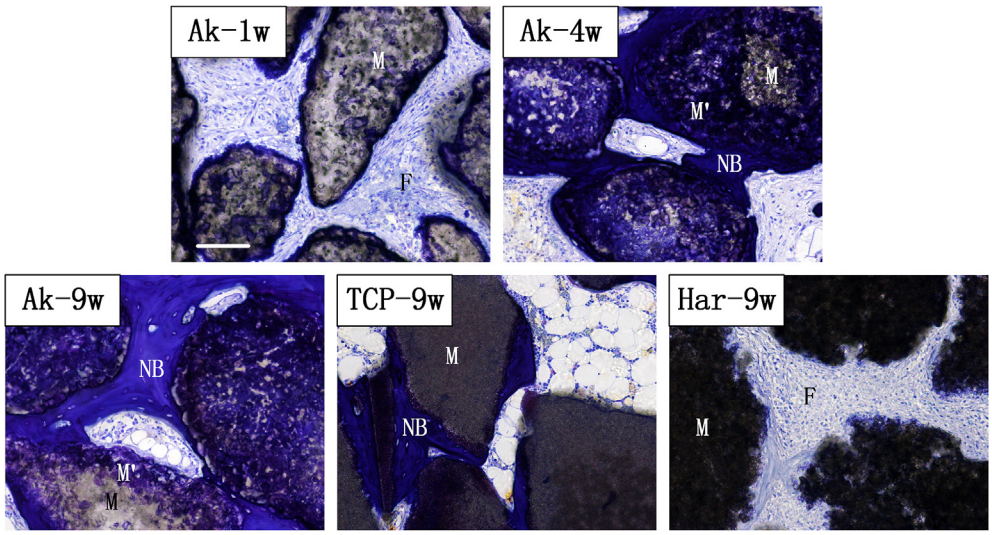

Fig. 6. Undecalcified toluidine blue staining during the osteoporotic bone defect regeneration process. Implant materials (M) appeared gray; new bone (NB) was stained blue (osteocyte lacunae can be clearly observed). M' represented the intermediate layer. Scale bar: 100 μm.

M' was indistinct after 4 weeks implantation. At time point of week 9, a greater material degradation proportion was observed in the Ak group than in Har and β-TCP groups.

3.7. Elemental distributions

Elemental distributions at material-bone junctions were displayed in Fig. 7. Generally, the direction for EDX linear scanning should pass through material regions to new bone regions, so that the elemental distribution from the original implant site to the novel bone site were recorded. The characteristic element of remaining Ak was “Si”. The formation of an “apatite” deposition at material original regions (denoted by “*”) can be identified by the emerging P peaks. New bone region was also rich in “P” and can be distinguished by the appearance of osteocyte lacunae. The results demonstrated that Si-rich regions were gradually replaced by P-rich deposition or new bone (Fig. 7; 4–9 weeks). Quantitative data indicated that the atom% of Mg and Si at material region was apparently decreased from week 4 (Mg: 6.28± 0.47%; Si: 13.79± 1.08%) to week 9 (Mg: 0.99± 0.12%; Si: 7.31± 0.73%). Characteristic Mg peaks of Ak become almost indistinguishable after 9 weeks, whereas Si peaks were still detectable at that time points.

4. Discussion

Insufficient osteogenesis between osteoporotic bone and endosseous implants usually results in poor biological fixation and it is one of challenging topics for material scientists to design proper orthopaedic biomaterials with biological functions for osteoporosis patients [22]. Currently, there's no approved biomaterial that was specifically appropriate for the application in osteoporotic bone clinically [23].

Beneficial ions adulteration is one of the commonly used approaches to improve the applicability of biodegradable material by adding new properties which adapt them to specific conditions. As an essential trace element of human beings, 60% of magnesium in human body is stored in bone, and 40% of them is exchangeable [24]. Deficiencies of Mg results in increased osteoclasts activity [25], reduced osteoblasts activity [26] and less perfect crystal in bone mineral in osteoporotic women [27], consequently accelerating bone loss [28]. Low magnesium level also affects the secretion of parathyroid hormone (PTH) and promotes mild inflammation, which indirectly contributes to osteoporosis [29]. Clinically, magnesium intake is positively correlated with bone mass content in pre and postmenopausal women [30,31], whereas high magnesium intake also significantly increases the risk of wrist fractures in postmenopausal women [32]. In that case, an appropriate and controllable Mg intake (*e.g.* from the released implants) is required.

In material science, Mg-containing biomaterials display potential applications as orthopaedic implants. Magnesium-based alloys show eminent biocompatible, osteoconductive and biodegradable properties [33]. The structural stability of $CaSiO_3$ is enhanced by magnesium adulteration. Also, the adhesion and proliferation properties of osteoblast on material surface could be directly stimulated by Al_2O_3 with Mg adulteration [34]. Most of these studies ascribe the beneficial effect of these Mg-containing biomaterials to the released Mg^{2+} (or other ions) [18]. However, we previously noticed that the released ions may also significantly change the microenvironmental pH through *in vivo* implants biodegradation, and a weak alkaline μe-pH was associated with greater new bone regeneration under an osteoporotic condition. We believe that both μe-pH elevation and the released Mg^{2+} are vital factors, whereas the *in vivo* detection of μe-pH change after implantation of these materials has not been realized yet.

Previously, we have demonstrated that the i-pHs on the materials surface were appreciably different from that of the bulk medium *in vitro* [3]. After biomaterials implantation, due to the complexity of *in vivo* situation which is influenced by both material surface properties and the blood/tissue fluid circulation, it is greatly necessary to make the direct monitoring of implants surface pH rather than theatrically prediction. In the present study, silicate based Mg-containing akermanite was fabricated and employed to rehabilitate the osteoporotic bone defect, and the detection of μe-pHs at different time points after Ak implantation was conducted by our previously established method [5]. The results indicated that, compared with β-TCP and Blank, Ak implantation immediately generated a higher μe-pH, and this alkaline condition would be maintained till 9 weeks. The initial μe-pH of Har was similar to Ak, while then decreased to a relatively lower level after week 1.

Previous studies have demonstrated that Ak exhibited better bone regenerative performance both *in vivo* and *in vitro* [17], while the present study further expanded this conclusion in the circumstances of OVX-induced osteoporotic conditions. In osteoporotic conditions, fibrous tissue encapsulation diminished and

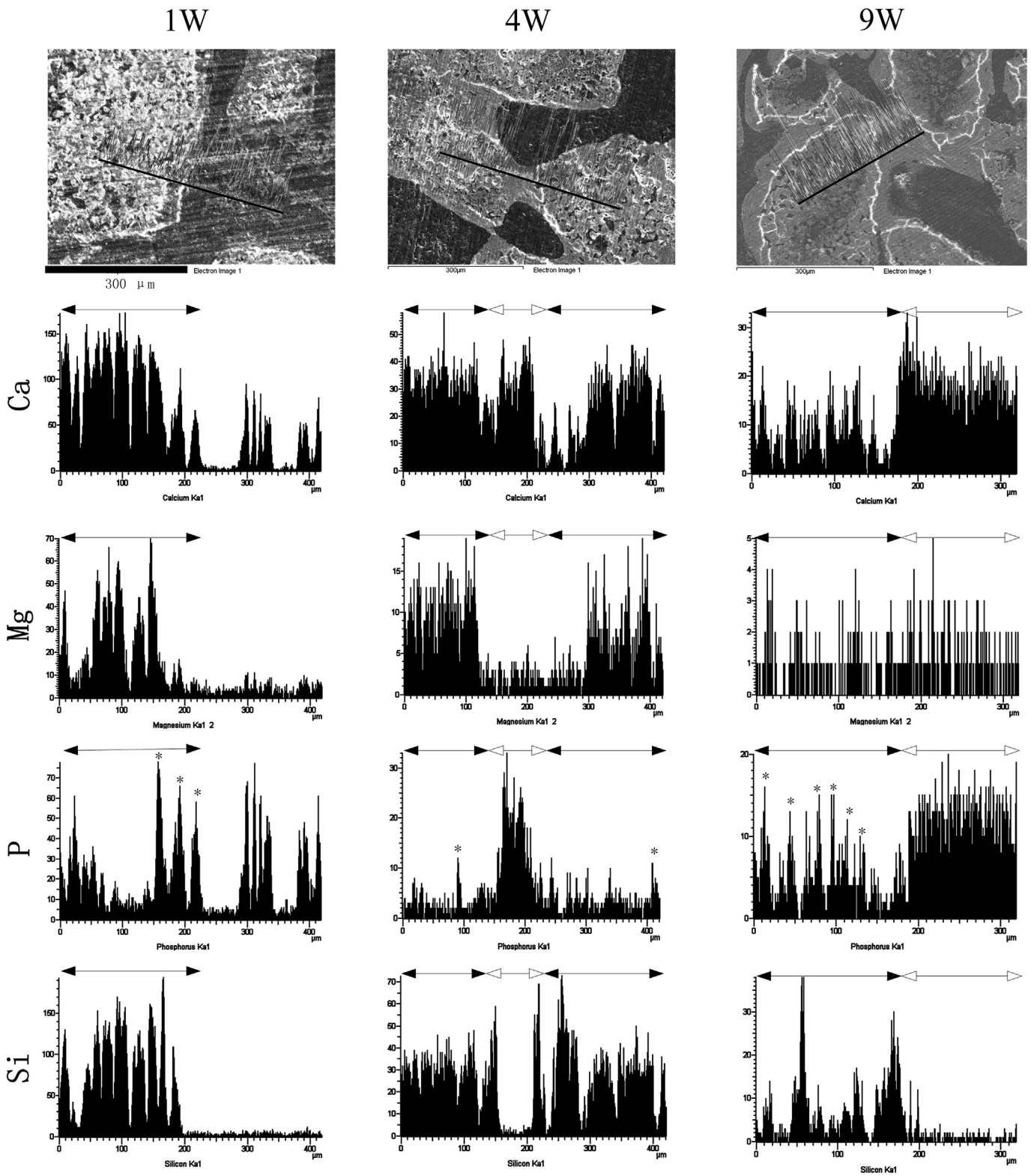

Fig. 7. Representative EDX line scans across Ak implantation sites. Scan tracks were labeled within black lines on SEM images. In elemental distribution histogram, the original material areas were labeled with black solid arrow, while new bone areas were labeled with hollow arrow. P peaks at material original regions were marked with "*". Scale bar: 300 μm.

disappeared within 4 weeks after Ak implantation. At week 9, new bone formation in Ak was respectively 94% and 261% higher than that in β-TCP and Har (Fig. 4). Anabolic osteoid formation activity was greater for Ak in comparison with β-TCP or Har, indicating increased osteoblast activity under those same conditions. Considering that weak alkaline conditions showed positive effects on osteoblastic differentiation from osteoporotic bone marrow stromal cells [5], we proposed that the better performance of Ak in the

treatment of osteoporotic bone defect may be not only ascribed to the anabolic effect of the Mg^{2+} but also its durable alkaline μe-pH.

The leverage of Bioglass® is attributed to its capability of forming a hydroxyapatite-like layer on its surface, promoting the binding between implants and bone [35]. By incorporating of Mg into silicate framework, diopside [36] and Akermanite [37] are reported to show hydroxyapatite formation ability in simulated body fluid (SBF). In this study, an intermediate layer (without osteocyte lacunae) emerged at week 4 post-surgery (Fig. 6; M'), connecting new forming bones with original material particles. This intermediate layer was rich in phosphorus (Fig. 7), indicating the formation of a calcium phosphate deposition. In addition, ions releasement could be speculated by the decreased content of Mg and Si at materials original regions, so that the released ions may take effect on the regeneration microenvironment by influencing cell behaviors as well as participating in the formation of new mineral. At last, among series biodegradable silicate-based materials, the incorporation of Mg/Zn into silicate framework slowed down the fast dissolution rate of CS [5], while the degradation rate and relative surface areas of Ak was still higher than that of Har (Fig. 3).

It is worth noticing here that, although the μe-pH was increased after Ak implantation, the influence of its effect on bone regeneration was still needed to be further confirmed. This is because the concentration of specific ions and protons in the microenvironment may interact with each other and it is impossible to design a biomaterial which only differs in μe-pH while the composition remains identical. That is to say, change in μe-pH may be an intermediate factor that different materials could generate a similar *in vivo* μe-pH from both their surface chemistry properties and interaction with the surrounding tissues. Furthermore, difficulties are still remained in respect of *in vivo* analysis for [Mg^{2+}], [SiO_3^{2-}], [Ca^{2+}] and so on.

To conclude, this study provided new insights into the beneficial effect of Ak on osteoporotic bone regeneration. In order to facilitate the development of novel orthopedic materials used for osteoporosis patients, further study on how μe-pH influences bone cells behaviors are still needed.

5. Conclusion

In the present study, akermanite was demonstrated to exhibit better bone regenerative performance in osteoporotic bone defect healing process than β-TCP and Har; and its better performance may be doubly attributed to the release of beneficial ions (*e.g.* Mg^{2+}) and a durable weak alkaline μe-pH it had generated after implantation.

Acknowledgments

This work was supported by grants from the National Natural Science Foundation of China (No. 51272274; 81672227; 51372170); Shenzhen Peacock Program (No. 110811003586331); Shenzhen Science and Technology Research funding (No. CXZZ 20150401152251209; JSGG20151030140325149; JSGG20150331 154931068, CXZZ20140417113430716) and partially from Hong Kong General Research Fund.

Appendix A. Supplementary data

Supplementary data related to this article can be found at http://dx.doi.org/10.1016/j.bioactmat.2016.11.004.

References

[1] O. Johnell, J.A. Kanis, An estimate of the worldwide prevalence and disability associated with osteoporotic fractures, Osteoporos. Int. 17 (2006) 1726–1733.
[2] X. Feng, J.M. McDonald, Disorders of bone remodeling, Annu. Rev. Pathol. 6 (2011) 121–145.
[3] Y.H. Shen, W.C. Liu, K.L. Lin, H.B. Pan, B.W. Darvell, S.L. Peng, et al., Interfacial pH: a critical factor for osteoporotic bone regeneration, Langmuir 27 (2011) 2701–2708.
[4] Y.H. Shen, W.C. Liu, C.Y. Wen, H.B. Pan, T. Wang, B.W. Darvell, et al., Bone regeneration: importance of local pH-strontium-doped borosilicate scaffold, J. Mater Chem. 22 (2012) 8662–8670.
[5] W. Liu, T. Wang, C. Yang, B.W. Darvell, J. Wu, K. Lin, et al., Alkaline biodegradable implants for osteoporotic bone defects-importance of microenvironment pH, Osteoporos. Int. 27 (2016) 93–104.
[6] K.L. Lin, L.G. Xia, H.Y. Li, X.Q. Jiang, H.B. Pan, Y.J. Xu, et al., Enhanced osteoporotic bone regeneration by strontium-substituted calcium silicate bioactive ceramics, Biomaterials 34 (2013) 10028–10042.
[7] Z.J. Li, X.N. Gu, S.Q. Lou, Y.F. Zheng, The development of binary Mg-Ca alloys for use as biodegradable materials within bone, Biomaterials 29 (2008) 1329–1344.
[8] S.L. Peng, G.Q. Zhou, K.D.K. Luk, K.M.C. Cheung, Z.Y. Li, W.M. Lam, et al., Strontium promotes osteogenic differentiation of mesenchymal stem cells through the Ras/MAPK signaling pathway, Cell Physiol. Biochem. 23 (2009) 165–174.
[9] C.T. Wu, J. Chang, W.Y. Zhai, A novel hardystonite bioceramic: preparation and characteristics, Ceram. Int. 31 (2005) 27–31.
[10] S. Xu, K. Lin, Z. Wang, J. Chang, L. Wang, J. Lu, et al., Reconstruction of calvarial defect of rabbits using porous calcium silicate bioactive ceramics, Biomaterials 29 (2008) 2588–2596.
[11] C. Wang, K.L. Lin, J. Chang, J. Sun, Osteogenesis and angiogenesis induced by porous beta-CaSiO3/PDLGA composite scaffold via activation of AMPK/ERK1/2 and PI3K/Akt pathways, Biomaterials 34 (2013) 64–77.
[12] S.Y. Ni, J. Chang, In vitro degradation, bioactivity, and cytocompatibility of calcium silicate, dimagnesium silicate, and tricalcium. Phosphate bioceramics, J. Biomat. Appl. 24 (2009) 139–158.
[13] C. Wu, J. Chang, Degradation, bioactivity, and cytocompatibility of diopside, akermanite, and bredigite ceramics, J. Biomed. Mater. Res. Part B-Appl. Biomat. 83B (2007) 153–160.
[14] T. Kokubo, Bioactive Glass-Ceramics - Properties and Applications Biomaterials, 12, 1991, pp. 155–163.
[15] Q.H. Liu, L. Cen, S. Yin, L. Chen, G.P. Liu, J. Chang, et al., A comparative study of proliferation and osteogenic differentiation of adipose-derived stem cells on akermanite and beta-TCP ceramics, Biomaterials 29 (2008) 4792–4799.
[16] C.T. Wu, J. Chang, S.Y. Ni, J.Y. Wang, In vitro bioactivity of akermanite ceramics, J. Biomed. Mater. Res. Part A 76A (2006) 73–80.
[17] Y. Huang, X. Jin, X. Zhang, H. Sun, J. Tu, T. Tang, et al., In vitro and in vivo evaluation of akermanite bioceramics for bone regeneration, Biomaterials 30 (2009) 5041–5048.
[18] L.G. Xia, Z.L. Yin, L.X. Mao, X.H. Wang, J.Q. Liu, X.Q. Jiang, et al., Akermanite bioceramics promote osteogenesis, angiogenesis and suppress osteoclastogenesis for osteoporotic bone regeneration, Sci. Rep. (2016) 6.
[19] P.P. Lelovas, T.T. Xanthos, S.E. Thoma, G.P. Lyritis, I.A. Dontasi, The laboratory rat as an animal model for osteoporosis research, Comp. Med. 58 (2008) 424–430.
[20] J.J. Westendorf, Osteoporosis: Methods and Protocols, Humana Press, Totowa, NJ, 2008.
[21] Y.H. An, K.L. Martin, Handbook of Histology Methods for Bone and Cartilage, Humana Press, Totowa, NJ, 2003.
[22] M. Fini, G. Giavaresi, P. Torricelli, A. Krajewski, A. Ravaglioli, M.M. Belmonte, et al., Biocompatibility and osseointegration in osteoporotic bone - a preliminary in vitro and in vivo study, J. Bone Jt. Surg.-Br. Vol. 83B (2001) 139–143.
[23] D. Arcos, A.R. Boccaccini, M. Bohner, A. Diez-Perez, M. Epple, E. Gomez-Barrena, et al., The relevance of biomaterials to the prevention and treatment of osteoporosis, Acta Biomater. 10 (2014) 1793–1805.
[24] J. Green, C.R. Kleeman, Role of bone in regulation of systemic acid-base-balance, Kidney Int. 39 (1991) 9–26.
[25] M.M. Belluci, T. Schoenmaker, C. Rossa, S.R. Orrico, T.J. de Vries, V. Everts, Magnesium deficiency results in an increased formation of osteoclasts, J. Nutr. Biochem. 24 (2013) 1488–1498.
[26] R.K. Rude, H.E. Gruber, Magnesium deficiency and osteoporosis: animal and human observations, J. Nutr. Biochem. 15 (2004) 710–716.
[27] L. Cohen, R. Kitzes, Infrared-spectroscopy and magnesium content of bone-mineral in osteoporotic women, Isr. J. Med. Sci. 17 (1981) 1123–1125.
[28] I. Zofkova, P. Nemcikova, P. Matucha, Trace elements and bone health, Clin. Chem. Lab. Med. 51 (2013) 1555–1561.
[29] S. Castiglioni, A. Cazzaniga, W. Albisetti, J.A.M. Maier, Magnesium and osteoporosis: current state of knowledge and future research directions, Nutrients 5 (2013) 3022–3033.
[30] Y.Q. Song, T.Y. Li, R.M. van Dam, J.E. Manson, F.B. Hu, Magnesium intake and plasma concentrations of markers of systemic inflammation and endothelial dysfunction in women, Am. J. Clin. Nutr. 85 (2007) 1068–1074.
[31] N. Saito, N. Tabata, S. Saito, Y. Andou, Y. Onaga, A. Iwamitsu, et al., Bone mineral density, serum albumin and serum magnesium, J. Am. Coll. Nutr. 23 (2004) 701s–703s.
[32] J.W. Nieves, Skeletal effects of nutrients and nutraceuticals, beyond calcium and vitamin D, Osteoporos. Int. 24 (2013) 771–786.
[33] M.P. Staiger, A.M. Pietak, J. Huadmai, G. Dias, Magnesium and its alloys as

orthopedic biomaterials: a review, Biomaterials 27 (2006) 1728–1734.
[34] H. Zreiqat, C.R. Howlett, A. Zannettino, P. Evans, G. Schulze-Tanzil, C. Knabe, et al., Mechanisms of magnesium-stimulated adhesion of osteoblastic cells to commonly used orthopaedic implants, J. Biomed. Mater Res. 62 (2002) 175–184.
[35] L.L. Hench, The story of bioglass (R), J. Mater Sci-Mater. M. 17 (2006) 967–978.
[36] S. Nakajima, Y. Harada, Y. Kurihara, T. Wakatsuki, H. Noma, [Physicochemical characteristics of new reinforcement ceramic implant], Shikwa Gakuho 89 (1989) 1709–1717.
[37] C.T. Wu, J. Chang, A novel akermanite bioceramic: preparation and characteristics, J. Biomat. Appl. 21 (2006) 119–129.